PHYSICAL REVIEW B VOLUME 49, NUMBER 19 15 MAY 1994-I

Response-function analysis of n^+-n-n^+ diode generators

V. Gružinskis, E. Starikov, and P. Shiktorov
Semiconductor Physics Institute, A. Goštauto 11, 2600 Vilnius, Lithuania

L. Reggiani
Dipartimento di Fisica ed Istituto Nazionale di Fisica della Materia, Universitá di Modena, Via Campi 213/A, 41100 Modena, Italy

L. Varani*
Centre d'Electronique de Montpellier, Université des Sciences et Techniques du Languedoc, 34095 Montpellier Cedex 5, France

(Received 26 July 1993)

We propose a response-function formalism to investigate electronic transport in semiconductor devices. To this end, a closed hydrodynamic approach coupled with the Poisson equation for the self-consistent electric field is used to simulate the stationary and transient characteristics of near micrometer n^+-n-n^+ InP diodes. The response functions of the local electric field and applied voltage are calculated by means of a procedure which is based on the response of the device to an impulsive current perturbation. The good agreement achieved with available experiments validates the present theoretical approach which suggests spatial negative differential mobility as the physical mechanism responsible for microwave generation. A significant increase of the cutoff frequency of the microwave power generation up to 600–700 GHz is predicted for submicrometer GaAs and InP diodes.

I. INTRODUCTION

Modern semiconductor devices based on hot-carrier transport are characterized by small size and, as a consequence, by strongly inhomogeneous distributions of electric field, carrier concentration, drift velocity, mean energy, etc. Under these conditions, transport in submicrometer structures differs significantly from transport in bulk materials and/or supermicrometer devices. Therefore, in recent years considerable efforts have been devoted to the theoretical investigation of short n^+-n-n^+ diodes, which can be considered one of the basis structures for modern microelectronics. In particular, the fundamental features of these diodes, including ballistic effects,[1,2] spatial distributions of various physical quantities,[3,4] small-signal-impedance behavior,[5] etc., have been the subject of deep studies. In addition, special attention has been paid to the theoretical analysis of microwave power generation in GaAs and InP diodes in order to estimate the attainable maximum generation frequency.[6–11] However up to now there has been no general consensus in the literature as concerns the maximum frequency and the mechanisms which are responsible for generation in submicrometer diodes.

For a theoretical analysis of transport and carrier heating in submicrometer structures, in addition to the knowledge of large- and small-signal transport coefficients,[12–19] it is important to obtain information about the separate roles which each part of the device (e.g., contacts, $n-n^+$ homojunctions, low- and high-field areas, etc.) play in determining the above coefficients. Such information can provide deep insight into the physical phenomena which causes microwave power generation. However this information is often given as phenomenological local parameters, such as differential mobility, diffusion coefficients, etc., which lack rigorous definitions in the presence of strong-field gradients.

The aim of this paper is to overcome the lack of rigor by constructing a theoretical approach based on the response-function formalism for the local electric field and applied voltage. This formalism provides a microscopic analysis of the relevant time scales associated with scattering mechanisms and interparticle interaction (here we consider long-range Coulomb interaction); thus it represents the ideal framework to physically analyze the characteristics and performances of modern electronic devices. As application, the case of n^+-n-n^+ diode generators made by III-V compounds is considered because of its practical interest. We remark that the theory so elaborated is a natural extension of the impedance-field method originally proposed by Shockley, Copeland, and James,[20] and further developed in Ref. 21.

The content of the paper is organized as follows. The theory is developed in Sec. II. The application to the case of near-micrometer InP diodes and some extension to submicrometer structures is reported in Sec. III. Some conclusions are given in Sec. IV.

II. THEORY

We consider a one-dimensional n^+-n-n^+ structure driven by a constant-current operation mode. Experimentally, such a mode of operation can be realized when the diode resistance is considerably smaller than the total resistance of the external circuit. The transient and stationary characteristics of the diode are obtained from a closed hydrodynamic approach based on a system of conservation equations for carrier number, drift velocity, and

0163-1829/94/49(19)/13650(7)/$06.00 ©1994 The American Physical Society

mean energy coupled with the Poisson equation previously developed by the authors.[10] The numerical simulation of the current-driven operation is implemented by solving an additional differential equation for the voltage drop U_d between the diode terminals:

$$\frac{d}{dt}U_d(t)=\frac{l}{\epsilon_0\epsilon_r}[j(t)-j_c(t)] , \quad (1)$$

where l is the total length of the diode, ϵ_r the relative static dielectric constant of the material, ϵ_0 the vacuum permittivity, $j(t)$ the total current density, and $j_c(t)$ the conduction current density which flow through the diode. (Here and hereafter quantities such as impedance, field impedance, etc. are normalized to unit cross-sectional area). Let us consider a stationary state of the diode characterized by a potential drop U_d^0 and a total current density j_0. Then, at a given initial time $t=0$, an impulsive δ-like perturbation of the total current density, δj_0, is introduced. By integrating Eq. (1), keeping in mind that any perturbation of the carrier concentration and velocity is initially absent, one obtains an initial perturbation of the voltage drop in the form $\delta U_d^0=\delta j_0(l/\epsilon_r\epsilon_0)$. The voltage perturbation leads to a homogeneous perturbation of the electric field inside the diode $\delta E_0=\delta U_d^0/l$ which, in turn, causes a time variation of $j_c(t)$. As a result, U_d also begins to change in accordance with Eq. (1), and finally relaxes to the initial value U_d^0 (i.e., the voltage perturbation vanishes in time under the constant-current operation). A time-dependent response function of the applied voltage, $D_U(t)$, can thus be defined as

$$D_U(t)=\frac{\delta U_d(t)}{\delta j_0}=\frac{l}{\epsilon_r\epsilon_0}\frac{\delta U_d(t)}{\delta U_d^0} . \quad (2)$$

To investigate the spatial profile of the voltage response, we also evaluate the response function of the local electric field in each point of the device, $D_E(t,z)$, defined as

$$D_E(t,z)=\frac{1}{\epsilon_r\epsilon_0}\frac{\delta E(t,z)}{\delta E_0} . \quad (3)$$

As follows from Eq. (3), the initial value $D_E(0,z)$ is proportional to the reciprocal geometrical capacitance per unit surface of the diode: $l/\epsilon\epsilon_0$, i.e., it is constant throughout the device. Therefore, the condition for the response function to vary inside the diode is that its time evolution must be different at different points. By Fourier transforming Eqs. (2) and (3), one obtains the small-signal impedance of the whole device, $Z(f)$, and the impedance field $\nabla Z(f,z)$ at frequency f, respectively, as

$$Z(f)=\int_0^\infty D_U(t)\exp(-i2\pi ft)dt , \quad (4)$$

$$\nabla Z(f,z)=\int_0^\infty D_E(t,z)\exp(-i2\pi ft)dt . \quad (5)$$

It should be pointed out that the integration of Eqs. (3) and (5) throughout the diode gives Eqs. (2) and (4). This means that every point of the diode makes its own contribution to the small-signal impedance, and these contributions are cumulative. Such a property is very important for a detailed analysis of the physical processes responsible for the diode performances.

III. APPLICATIONS

The above theory is applied to near-micrometer n^+nn^+ InP diodes. The main parameters used are given by $n^+=10^{18}$ cm^{-3}, $n=1.5\times10^{16}$ cm^{-3}, and the n-region length $l_n=1.0$ μm. These diodes have been investigated experimentally by Rydberg,[22,23] and a wide-band generation in the frequency range $110<f<220$ GHz with a maximum power of about 10 mW has been obtained for applied voltages in the range between 4.6 and 6.0 V. To analyze the high-frequency performance of these diodes, one should recall that a considerable role is played by drift-velocity overshoot,[6] which increases the difference between maximum and minimum drift velocities inside the n region, and strengthens the usual Gunn effect. This is illustrated in Figs. 1(a)–1(d), which present a stationary profile of carrier concentration, drift velocity, mean energy, and electric field for a diode with abrupt homojunctions, and cathode and anode lengths, respectively, of $l_1^+=0.05$ μm and $l_2^+=0.1$ μm, under an applied voltage $U_d^0=5$ V. These results agree within a few percent at worst with those obtained by an analogous simulation performed with an ensemble Monte Carlo method.[24] Figure 1(b) shows the appearance of a velocity-overshoot region when the thermal electrons enter from the cathode n^+ region into the n region, where a high electric field is present. The profile of the velocity overshoot consists of a rapid increase of the drift velocity followed by a relatively slow decrease. The former behavior is caused by the initial ballistic motion of carriers in the momentum and real spaces. The latter is due to the transfer of carriers into the upper valleys which implies both a randomization of the instantaneous velocity component in the direction of the applied field, and a reduction of the drift velocity due to a higher effective mass. The decrease of the drift velocity inside the diode is accompanied by an increase of the carrier concentration and the electric field, which reaches its maximum value near the anode. Therefore, there exists a kind of negative differential mobility (NDM) in the space region $0.3<z<1.0$ μm, where the drift velocity decreases with increasing electric fields. Furthermore, a space region between the cathode and the maximum value of the drift-velocity overshoot is needed for the average energy to reach the value necessary for the onset of the electron transitions to the upper valleys. Such a space region is usually called the dead zone,[25] and in our case it extends for about 0.25 μm starting from the n^+n homojunction. The remaining part of the n region, where the drift velocity as a function of space exhibits a negative slope, can be considered as the active zone of the diode. The main features of the microwave power generation are determined primarily by the physical processes which occur in this region.

The general scenario for transit-time oscillations due to velocity overshoot is similar to that for the usual bulk Gunn effect. Because of the spatial negative differential mobility (SNDM), a spontaneous fluctuation of the carrier concentration can grow in time, leading to the formation of an accumulation layer in the diode region characterized by a decreasing profile of the drift velocity. Then the propagation of the layer toward the anode leads to the appearance of time variations of the conduction

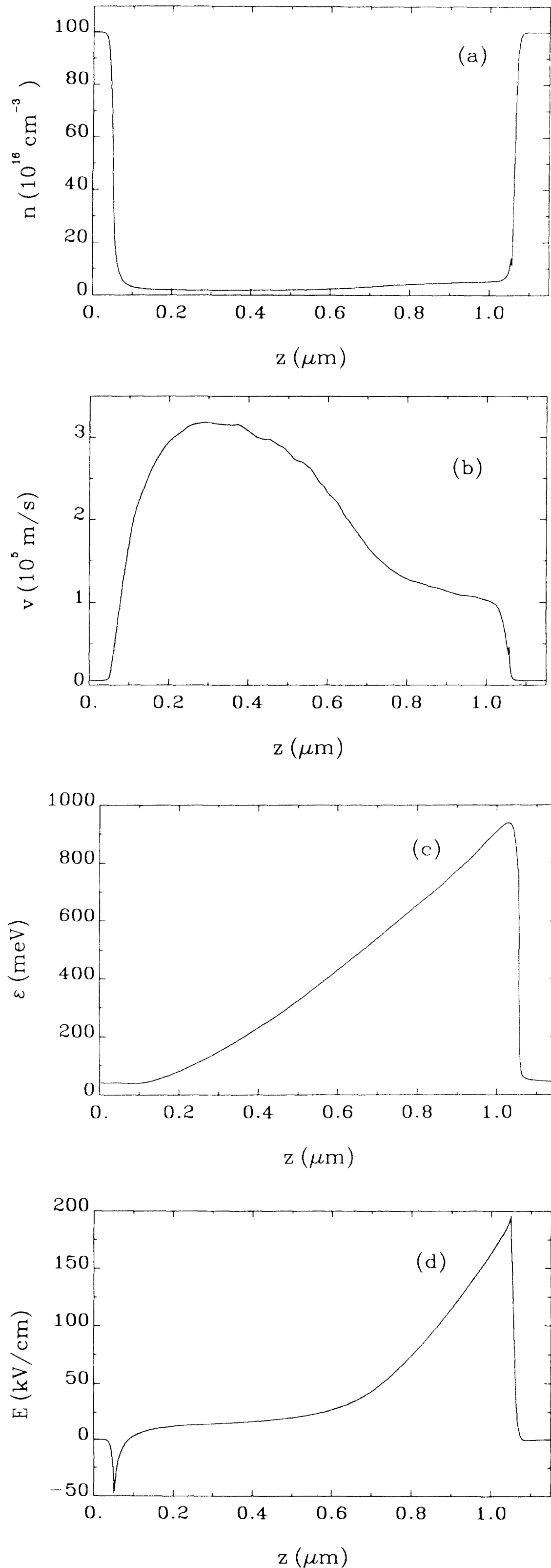

FIG. 1. (a) Concentration, (b) drift velocity, (c) average energy, and (d) electric-field profiles in the n^+-n-n^+ InP diode at 300 K calculated at $U_d^0=5$ V. Diode parameters: $n^+=10^{18}$ cm^{-3} and $n=1.5\times10^{16}$ cm^{-3}, and cathode, n-region, and anode lengths, respectively, of 0.05, 1.0, and 0.1 μm with abrupt homojunctions.

current in the diode or of the total current in the external circuit. When the layer leaves the diode, a redistribution of the internal electric field takes place and the appearance of the SNDM starts up again. Thus the process of a layer formation, its transport across the diode, and its disappearance at the anode assumes a periodic character which is at the basis of microwave generation.

The mechanism just outlined has evident advantages with respect to the NDM of the usual Gunn effect. These are as follows.

(i) The cutoff frequency for SNDM in short diodes can be much greater than that for NDM in long diodes because of the dynamic character of the SNDM formation. Moreover, in principle, generation can be obtained in materials which do not exhibit steady-state NDM such as n-Si[6]

(ii) The maximum value of the drift velocity in SNDM can be about 2–4 times greater than that in NDM. This leads to a higher transit-time velocity and to a larger peak-to-valley ratio in short rather than long diodes.

(iii) The SNDM causes the formation of an accumulation layer instead of a dipole domain. This also represents a favorable condition for improving the high-frequency performance of microwave power generator.[26]

The above advantages are naturally in favor of a significant improvement of the conversion efficiency, a shortening of the time necessary for the layer formation and its transit across the active region, and a general improvement of the diode performances at increasing lattice temperatures. It should be stressed that, in materials which exhibit the Gunn effect (e.g., n-GaAs and n-InP), by reducing the diode length one ensures a continuous transition from the static NDM to the dynamic SNDM. We conclude that the Gunn effect and the dynamic SNDM strengthen each other in passing from long to submicrometer diodes.

Figure 2 shows the time dependence of the response function of the local electric field calculated for $U_d^0=5$ V at several points of the diode with coordinates, as measured from the cathode terminal, respectively, at $z=0.03$, 0.25, 0.45, 0.65, 0.85, and 1.03 μm. The first

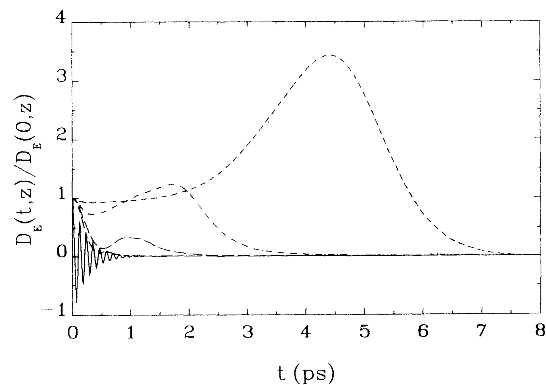

FIG. 2. Normalized response functions of the local electric field as a function of time for $U_d^0=5$ V under current-driven operation at different points inside the diode of Fig. 1 as measured from the cathode terminal: $z=0.03$, 0.25, 0.45, 0.65, 0.85, and 1.03 μm (solid, short-long-dashed, long-dashed, dot-dashed, dotted, and short-dashed lines).

point is placed inside the cathode. Here the response function exhibits a plasma-oscillation pattern which is damped by the collision time. The same pattern is found inside the anode. The second point corresponds in space to the maximum value of the drift-velocity overshoot. Here the response function is found to decay nearly exponentially on the time scale of momentum relaxation. For the other points, which are placed between the maximum value of the drift-velocity overshoot and the anode, the response function exhibits a pronounced bell-shaped tail. The maximum value of the bell shape and its corresponding time is found to increase by increasing the coordinate along the diode up to the point where the carrier mean energy has its highest value (the short-dashed curve in Fig. 2). Then the maximum of the bell-shaped tail begins to decrease rapidly, and vanishes at the beginning of the anode region. The time evolution of the perturbed carrier concentration, $\delta n(t,z)=n(t,z)-n_0(z)$ [$n_0(z)$ being the stationary profile corresponding to $U_d^0=5$ V], is illustrated in Fig. 3. The initial perturbation of the applied voltage and, hence, of the electric field inside the diode, leads to the appearance of a space-charge wave which is located in the active region of the diode (solid curve, $t=1$ ps). Then this wave turns in an accumulation layer followed by a narrow depletion region near the anode (the short-dashed curve, $t=2$ ps). By comparing with Fig. 2, one can conclude that the accumulation layer is formed in the region of the diode where the negative slope of the drift velocity as a function of space is maximum. After its formation, which takes about 2 ps, the accumulation layer begins to propagate toward the anode. The layer disappears, reaching the anode with a negative value of δn. Therefore, the bell-shaped pattern of $D_E(t,z)$ is related to the movement and growth of the layer inside the diode, as well as to its vanishing at the anode.

Figure 4 reports the voltage response function at increasing values of the applied voltage. The numbers on the curve correspond to the applied voltage in volt units.

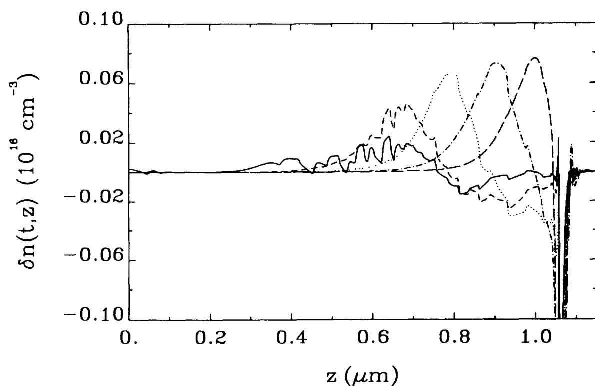

FIG. 3. Concentration perturbation $\delta n(t,z)=n(t,z)-n_0(z)$ with respect to the stationary concentration profile $n_0(z)$ as a function of the coordinate z along the n^+-n-n^+ diode calculated under current-driven operation at various times $t=1$, 2, 3, 4, and 5 ps after the voltage perturbation (solid, short dashed, dotted, dot-dashed, and long-dashed lines, respectively). $U_d^0=5$ V and, $\delta U_0=0.05$ V.

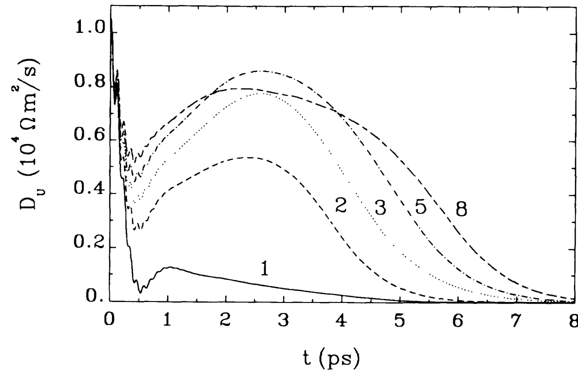

FIG. 4. Voltage response function as a function of time calculated under current-driven operation for the diode of Fig. 1. The numbers labeling the curves correspond to the magnitude of the applied voltage in V units.

(Of course, being under current-driven operation, all curves are calculated at fixed current densities j_0 corresponding to the given U_d^0.) The general shape of each curve is similar, and can be analyzed in terms of short- and long-time behaviors. At short times we find a sharp decrease of $D_U(t)$ which is modulated by the plasma oscillations associated with the n^+ regions. (By comparison with Fig. 2, one can conclude that the plasma oscillations are caused by the n^+ regions only.) This decrease of $D_U(t)$ comes from the contribution of the electrons, which are placed in the dead zone of the n region. At long times we find a bell-shaped behavior, analogous to that of $D_E(t,z)$, which is caused by the propagation of the accumulation layer across the diode, and which is more pronounced the higher the applied voltage. When the propagation of the accumulation layer is terminated, the voltage response function vanishes.

The bell-shaped behavior of the voltage response function is responsible for the appearance of one or more minima in the frequency spectrum of the real part of the small-signal impedance of the diode, $\mathrm{Re}[Z_d(f)]$. This is illustrated in Fig. 5, where the spectra of $\mathrm{Re}[Z_d]$ are presented for $U_d^0=5$ and 8 V (solid and dashed curves, respectively). In the frequency range where $\mathrm{Re}[Z_d(f)]<0$,

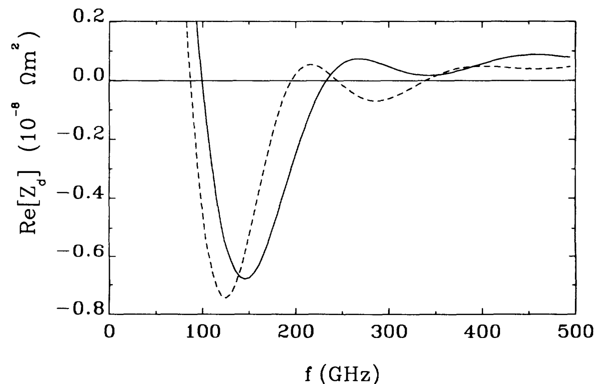

FIG. 5. Frequency dependence of the real part of the small-signal impedance for $U_d^0=5$ and 8 V (solid and dashed lines, respectively).

an amplification and generation of the microwave power is possible. The frequency regions corresponding to negative values of Re$[Z_d]$ are plotted in Fig. 6 as a function of the applied voltages. These regions, whose boundaries are shown by continuous lines, define the amplification bands in the (f, U_d^0) plane. In each band the dashed line corresponds to the frequency at which Re$[Z_d]$ is at a minimum. It should be remarked that we find a second generation band at voltages higher than 5 V. (In general, more bands can appear at sufficiently high voltages.) The frequency region where Re$[Z_d]$ is negative ranges from 90 to 240 GHz for $4.5 \leq U_d^0 \leq 6$ V, and agrees well with the experimental values for microwave generation.[22,23]

For a more detailed analysis of the contribution which the various regions of the diode make to the total small-signal impedance, Fig. 7 reports the spatial profile of the real part of the impedance field, Re$[\nabla Z]$, calculated, respectively, at frequencies $f = 100$, 150, 200, and 250 GHz for $U_d^0 = 5$ V. It should be emphasized that, at frequencies lower than 70 GHz, Re$[\nabla Z]$ is found to be positive everywhere, in spite of the fact that the drift velocity has a negative slope in the active region. This result reflects the dynamic nature of the high-frequency instabilities in transit-time diodes. From Fig. 7, we see that the local differential resistance is independent of frequency in the dead zone, while becoming dependent on it only in the active region of the diode (i.e., for $0.3 < z < 1.05$ μm). Moreover, in the dead zone the imaginary part of the impedance field, Im$[\nabla Z]$, is found to be equal to zero at all frequencies. In other words, from the electrical point of view, the dead zone can be considered as a real positive resistance without any imaginary part. Thus all current instabilities are caused by the active zone only.

To understand the spatial behavior of the impedance field in the active zone, let us come back to the physical meaning of this quantity. By definition, the impedance field at frequency f and point z is given by the ratio of the Fourier component of the local electric field $E_f(z)$ to the Fourier component of the total current at the same frequency. In the active zone of the diode, the spatial dependence of $E_f(z)$ is proportional to $\exp[ik(f)z]$ (i.e., it can be represented as a growing space wave), where the

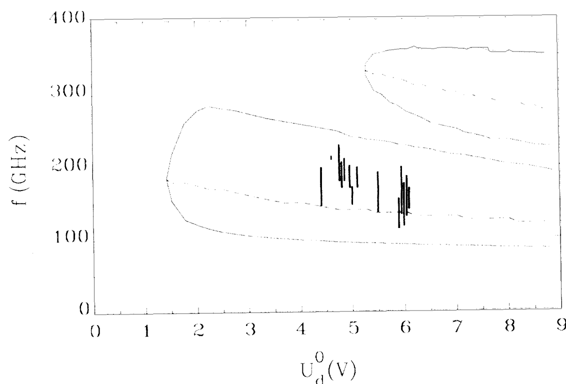

FIG. 6. Amplification bands for the n^+-n-n^+ InP diode of Fig. 1. The dashed lines show the optimal frequency corresponding to the maximum negativity of Re$[Z_d(f)]$. The vertical bars summarize the experimental data (Refs. 22 and 23).

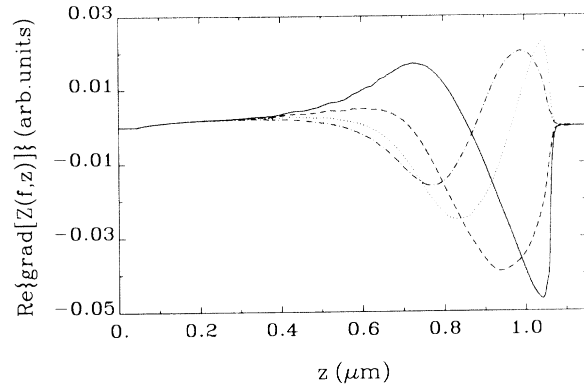

FIG. 7. Real part of the impedance field as a function of the spatial coordinate at the frequencies $f = 100$, 150, 200, and 250 GHz (solid, dashed, dotted, and dot-dashed lines, respectively). $U_d^0 = 5$ V.

real and imaginary parts of $k(f)$ determine the wavelength and spatial increase respectively, of the space wave. Therefore, the curves in Fig. 7 correspond to growing space waves of the local electric field which start at the beginning of the active zone and vanish at the anode contact. From the same figure it is also evident that the wavelength of the space waves decreases at increasing frequency. Indeed, at sufficiently high frequencies more than one minimum can appear in the active region.

Figure 7 also serves to individuate the regions of the diode which are responsible for generation in the intermediate frequency range $100 < f < 250$ GHz. In this range, all space waves of Re$[\nabla Z]$ have only one negative minimum in the active zone, and compose a single amplification band (see Figs. 5 and 6). The small-signal impedance of the diode reaches a maximum negative value near the frequency $f = 150$ GHz (see Fig. 5), when the whole region of the layer propagation (see Fig. 3) is responsible for such a negative value. At higher frequencies, the negative values of the small-signal impedance Re$[Z]$ decrease due to the appearance of a region with positive values of Re$[\nabla Z]$ near the anode contact. This has an interesting physical consequence. In order to shift the maximum of Re$[Z]$ to higher frequencies, it is necessary to decrease the diode length (i.e., to cut the near-anode region with positive values of Re$[\nabla Z]$ at high frequencies). For example, as follows from Fig. 7, for the frequency $f = 250$ GHz a reduction of the n region from 1.0 μm down to 0.85 μm should eliminate the positive Re$[\nabla Z]$ in the region near the nn^+ homojunction. Such an expectation is fully confirmed by direct Monte Carlo simulations of the reduced diode. Thus the information obtained from the impedance field calculations can be conveniently used for a proper choice of the diode length, doping profile, etc. A further possibility exists that additional minima of Re$[\nabla Z]$ are formed inside the active zone, being responsible for the appearance of upper amplification bands. For example, the second amplification band at frequencies $220 \leq f \leq 350$ GHz in Fig. 6 is caused by the appearance of a second minimum of Re$[\nabla Z]$ near the anode contact.

From the small-signal analysis, we provide an estimate for the values of the parameters of the external resonant circuit which are needed for generation. Accordingly, to obtain generation in the first band only, we find that the total resistance of the external circuit must be less than $7\times10^{-9}\ \Omega\,\mathrm{m}^2$ (which from Fig. 5 is the maximum value of $|\mathrm{Re}[Z_d]|$ in the first generation band). For a typical value of the cross-sectional area $A=10^{-9}\ \mathrm{m}^2$, this means that the load resistance of the device should not exceed the value of several Ω. The corresponding estimates for the external circuit inductance can be obtained from the frequency dependence of $\mathrm{Im}[Z_d]$.[24] The generated power and the efficiency of the diode generation in the series resonant circuit, which consists of the load resistance R and the inductance L, are reported in Figs. 8(a) and 8(b), respectively. The generated power $P_{\mathrm{gen}}(f)$ is evaluated as the alternative power extracted from the load resistance:

$$P_{\mathrm{gen}}=R(\overline{j^2}-\overline{j}^2) \tag{6}$$

where the bar means an average over a period. Accordingly, the efficiency η of the generation is calculated as

$$\eta=\frac{P_{\mathrm{gen}}}{P_{\mathrm{gen}}+\overline{P}}\ , \tag{7}$$

where $\overline{P}=\overline{j}U_a$ is the total power averaged over a period,

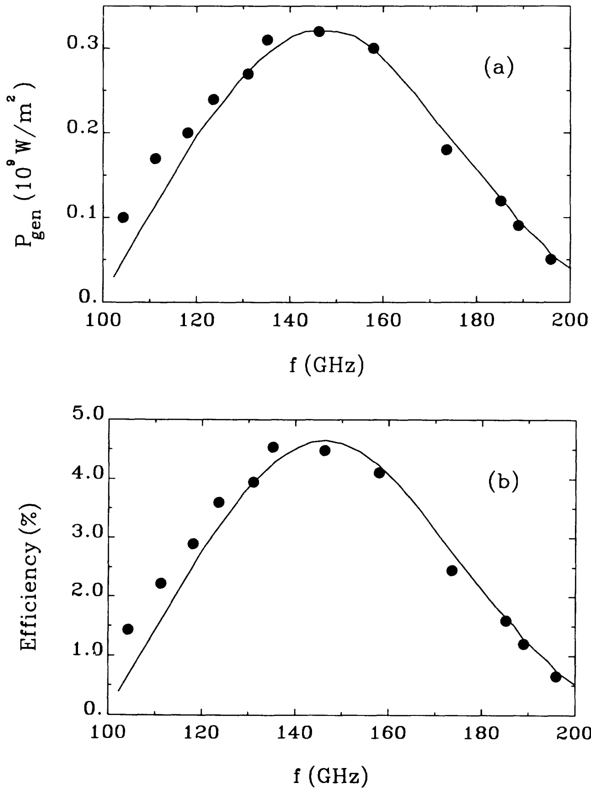

FIG. 8. (a) Generated power and (b) efficiency of the microwave power generation. Full curves refer to the present nonlinear hydrodynamic approach, and points to the kinetic approach performed using an ensemble Monte Carlo simulation. The parameters are the same as Fig. 1 with $n=2\times10^{16}\ \mathrm{cm}^{-3}$, $R=2.5\times10^{-9}\ \Omega\,\mathrm{cm}^2$, and the total applied voltage $U_a=7.5$ V.

and U_a the voltage applied to the whole circuit. Since $P_{\mathrm{gen}}\ll\overline{P}$, and $\overline{P}$ is a slowly varying function of frequency, the spectral behavior of the generated power is very similar to that of the efficiency. The main features of the microwave power generation are found to be in full agreement with the SNDM mechanism described above (see the discussion of Fig. 1). In particular, both Monte Carlo and hydrodynamic simulations show the formation of accumulation layers rather than dipole domains, and the low-frequency amplification band corresponds to the formation of a single accumulation layer. When the parameters of the resonant circuit are chosen in such a way as to operate in the second amplification band (see Fig. 6), we find two accumulation layers which move simultaneously along the diode.

The good agreement we have found between results for the hydrodynamic and kinetic approaches strongly supports the physical reliability of our modeling. In particular, calculations exhibit a maximum generation power at about 150 GHz, which compares well with experimental findings[22,23] where, for a variety of samples, such a maximum is found in the frequency range $110<f<220$ GHz. By assuming $A=10^{-9}\ \mathrm{m}^2$, we obtain a maximum theoretical value of the generated power $P_{\mathrm{gen}}=300$ mW at $f=150$ GHz, which should be compared with the maximum power of 7 mW measured experimentally at $f=180$ GHz.[23] This significative difference leads us to conclude that the output power of real devices can still be improved by appropriate choices of the resonator external parameters and/or technology refinements.

The overall agreement here found between calculations and available experiments for near-micrometer InP diodes validates our approach and allows us to extend it to the case of submicrometer n^+nn^+ GaAs and InP diodes at different temperatures. Some interesting results of the small-signal characteristics are presented in Fig. 9. Here the maximum and minimum frequencies for generation within the first band are plotted as functions of the

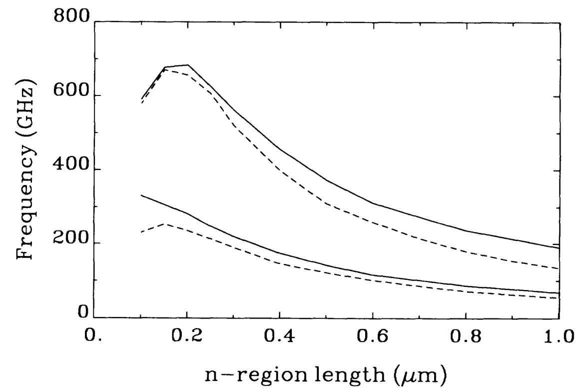

FIG. 9. Upper and lower frequencies of the first-generation band as a function of the length of the diode n region at $T=400$ K. Diode parameters: $n^+=10^{18}\ \mathrm{cm}^{-3}$, and $n=10^{17}\ \mathrm{cm}^{-3}$; the cathode and anode lengths are 0.05 and 0.25 μm, respectively, with an intermediate region of 0.1 μm between the n^+ and n regions with linear grading of the doping level. Continuous and dashed curves refer to the case of InP at $U_d^0=2.5$ V and GaAs at $U_d^0=1.5$ V, respectively.

n-region length for the case of GaAs and InP diodes at $T = 400$ K. We remark that the maximum generation frequency reaches values of 600–700 GHz when the n-region length reduces to 0.3–0.2 μm. These values are considerably higher than those obtained in bulk materials under static NDM. For shorter lengths we find a degradation of the frequency performances, which can be associated with the fact that the space charge penetrates the whole n region due to free-carrier diffusion.[27]

IV. CONCLUSIONS

Within the framework of a response-function formalism, we have presented a rigorous space and time analysis of the local electric field, and applied voltage in near-micrometer and submicrometer diode generators. These functions are found to provide a valuable physical insight of the different time scales and microscopic mechanisms describing the electronic processes. The spatial negative differential mobility (SNDM) associated with overshoot effects appearing when thermal electrons enter from the cathode n^+ region into the active n region is found to be an effective physical mechanism which improves considerably the high-frequency performance of submicrometer diodes, and strengthens the usual Gunn effect. From an analysis of different geometries and materials, we predict a maximum generation frequency of about 700 GHz in GaAs and InP diodes with lengths in the n region of about 0.2 μm.

ACKNOWLEDGMENTS

This work was supported by the Commission of European Community (CEC) in the framework of the Human Capital and Mobility program through Contract No. CIPA3510PL921499, by the Italian Consiglio Nazionale delle Ricerche (CNR), by a Soros Foundation Grant awarded by the American Physical Society, and by the Italian Ministero della Universitá e della Ricerca Scientifica e Tecnologica (MURST).

---

*On leave from Dipartimento di Fisica ed Istituto Nazionale di Fisica della Materia, Universitá di Modena, Via Campi 213/A, 41100 Modena, Italy.

[1] S. A. Trugman and A. J. Taylor, Phys. Rev. B **33**, 5575 (1986).
[2] H. U. Baranger and J. W. Wilkins, Phys. Rev. B **36**, 1487 (1987).
[3] D. L. Woolard, H. Tian, R. J. Trew, M. A. Littlejohn, and K. W. Kim, Phys. Rev. B **44**, 11 119 (1991).
[4] M. Nekovee, B. J. Geurts, H. M. J. Boots, and M. F. H. Schuurmans, Phys. Rev. B **45**, 6643 (1992).
[5] C. M. Krowne, Phys. Rev. B **37**, 891 (1987).
[6] M. R. Friscourt, P. A. Rolland, A. Cappy, E. Constant, and G. Salmer, IEEE Trans. Electron Devices **ED-30**, 223 (1983).
[7] M. Curov and A. Hintz, IEEE Trans. Electron Devices **ED-34**, 1983 (1987).
[8] A. E. Ekzhanov, A. S. Kosov, and V. A. Zotov in *Proceedings of the 20th European Microwave Conference,* Budapest, 1990 (Microwave Exhibition and Publishers, Tunbridge Wells, 1990), p. 1702.
[9] H. Tian, K. W. Kim, M. A. Littlejohn, U. K. Mishra, and M. Hashemi, J. Appl. Phys. **72**, 5695 (1992).
[10] C. Gružinskis, E. Starikov, P. Shiktorov, L. Reggiani, M. Saraniti, and L. Varani, Appl. Phys. Lett. **61**, 1456 (1992).
[11] K. F. Wu, J. Czekaj, and M. P. Shaw, J. Appl. Phys. **74**, 315 (1993).
[12] W. Shockley, Bell Syst. Techn. J. **33**, 799 (1954).
[13] M. Kurata, IEEE Trans. Electron Devices **ED-18**, 200 (1971).
[14] M. Reiser IEEE Trans. Electron Devices **ED-20**, 35 (1973).
[15] R. Bosch and H. W. Thim, IEEE Trans. Electron. Devices **ED-21**, 16 (1974).
[16] S. E. Laux, IEEE Trans. Electron. Devices **ED-32**, 2028 (1985).
[17] C. M. Krowne and P. A. Blakey, J. Appl. Phys. **61**, 2257 (1987).
[18] H. L. Grubin in *The Physics of Submicron Semiconductor Devices,* edited by H. L. Grubbin, D. K. Ferry and C. Jacoboni (Plenum, New York, 1988), p. 45.
[19] G. Ghione, M. Pirola and C. U. Naldi, in *Simulation of Semiconductor Devices and Processes,* edited by W. Fichtner and D. Aemmer (Hartung-Gorre-Verlag, Konstanz, 1991), Vol. 4, p. 71.
[20] W. Shockley, J. A. Copeland, and R. P. James in *Quantum Theory of Atoms, Molecules and Solid State,* edited by P. O. Lowdin (Academic, New York, 1966), p. 537.
[21] K. M. van Vliet, H. Friedman, R. J. J. Zijlstra, A. Gisolf, and A. van der Ziel, J. Appl. Phys. **46**, 1804 (1975).
[22] A. Rydberg, Int. J. Infrared Millimiter Waves **11**, 383 (1990).
[23] A. Rydberg, IEEE Electron. Device Lett. **11**, 439 (1990).
[24] V. Gružinskis, E. Starikov, P. Shiktorov, L. Reggiani, M. Saraniti, and L. Varani, in *Simulation of Semiconductor Devices and Processes,* edited by S. Selberherr, H. Stippel and E. Strasser (Springer-Verlag, Wien, 1993) Vol. 5, p. 149.
[25] V. Bareikis, K. Kibickas, J. Liberis, A. Matulionis, R. Miliusite, J. Parseliunas, J. Pozhela, and P. Sakalas in *High-Speed Electronics,* edited by B. Källbäck and M. Beneking (Springer-Verlag, Berlin, 1986), p. 28.
[26] M. I. Dyakonov, M. E. Levinshtein, and G. S. Simin, Fiz. Tekh. Poluprovodn. **15**, 2116 (1981) [Sov. Phys. Semicond. **15**, 1229 (1981)].
[27] L. Varani, T. Kuhn, L. Reggiani and Y. Perles, Solid-State Electron. **36**, 251 (1993).